

Computer simulation of performance characteristics of (GaIn)(NAs) diode lasers

ROBERT P. SARZALA

Institute of Physics, Technical University of Łódź, ul. Wólczańska 219, 93-005 Łódź, Poland.

Comprehensive self-consistent optical-electrical-thermal-gain modelling is used to enable structure optimization and to simulate room-temperature (RT) continuous-wave (CW) performance characteristics of (GaIn)(NAs) lasers emitting in the 1.3- μm wavelength range. The simulation takes into consideration all physical phenomena crucial for a laser operation including all important interactions between them.

1. Introduction

Telecommunication systems at the optical fiber window of 1.3 μm exhibit many advantages over their earlier 0.85 μm counterparts:

- the dispersion minimum of standard fibers corresponding to this wavelength raises available transmission rates,
- lower fiber absorption losses enable longer transmission distances,
- driving voltage is reduced to roughly two thirds of that used for 0.85 μm lasers,
- the issue of eye-safety may be quite decisive, since at 1.3 μm the human eye tolerates about ten times the optical power that would be dangerous at 0.85 μm .

Currently commercially available long-wavelength 1.3- μm diode lasers are based on (InGa)(AsP)/InP structures, often with GaAs/AlAs distributed-Bragg-reflector (DBR) mirrors. This construction requires a complicated growth and processing procedure which is probably too expensive for mass-produced commercial devices. Besides, since the above lasers exhibit poor temperature characteristics, mainly due to insufficient electron confinement, thermoelectric coolers are required in their practical use. Therefore, taking additionally into consideration the well established arsenide technology of GaAs/(AlGa)As/AlAs structures with GaAs/AlAs DBRs and oxidized AlAs layers), at present the most promising solution to this problem seems to be arsenide structures with such active-gain materials which are lattice matched to GaAs and emit in the 1.3 μm range. Then the whole structure could be grown in one epitaxial process which considerably reduces its cost and enables its mass manufacturing.

Possible candidates for such a gain material are GaAsSb quantum wells, InAs quantum dots and the new material $\text{Ga}_x\text{In}_{1-x}\text{N}_y\text{As}_{1-y}$, proposed first by KONDOW *et al.* [1], [2]. In the GaSb diode lasers, there are still some uncertainties concerning the

band line-up. Besides, their active layers operate under a very high compressive strain which may be a source of unwanted rapid degradation. Quantum-dot lasers, on the other hand, still exhibit low gain and a considerable increase in their threshold current at high temperatures. Therefore currently they should be considered as low-power room-temperature 1.3- μm emitters only.

The $\text{Ga}_x\text{In}_{1-x}\text{N}_y\text{As}_{1-y}$ material may be grown on GaAs. Its emission wavelengths are between 1.1 μm and nearly 1.6 μm and may be adjusted by changing the nitrogen content [3], [4]. Strictly speaking, both mole fractions x and y may be properly selected to obtain suitable both the lattice constant and the emission wavelength. Anyway, (GaIn)(NAs) material is a surprising candidate for the GaAs-lattice matched 1.3- μm gain region [1]. Contrary to the general rule of $\text{A}^{\text{III}}\text{B}^{\text{V}}$ materials, according to which decreasing lattice constant increases the band gap, the large electronegativity of N and its small size cause a very strong bowing parameter [1]. Therefore, the addition of N to GaAs or GaInAs dramatically decreases the band gap. Hence, fabrication of arsenide diode lasers with GaAs-lattice matched (GaIn)(NAs) active regions emitting at the 1.3- μm wavelength range becomes possible. There are also other advantages of the above solution. As compared to its counterparts, the (GaIn)(NAs) diode laser exhibits higher values of the T_0 parameter (describing temperature dependence of the threshold current), higher possible operating temperatures, higher efficiency and higher achievable output power. All these advantages follow from the higher values of electron effective mass (therefore the valence and the conduction band densities of states are better matched) and deeper conduction-band quantum wells providing better confinement for electrons [1], [5].

Edge-emitting (in-plane) 1.3- μm (GaIn)(NAs)/GaAs diode lasers have already been reported many times. Room-temperature continuous-wave operation at 1.3 μm wavelength has been reported for a device fabricated by molecular beam epitaxy (MBE) [6], [7] and metal organic chemical vapor deposition (MOCVD) [8]–[10]. The first distributed feedback (DFB) laser diodes at 1.3 μm have been demonstrated in the year of 2000 [11].

Despite strong progress in the development of device structures, many fundamental material parameters still remain unknown or not fully understood. There are many parameters not yet optimized for these devices. Nevertheless, they demonstrate the exciting potential of (GaIn)(NAs) on GaAs for low cost, long-wavelength VCSELs. The technology seems to be currently largely material and knowledge limited. Extension to longer wavelengths, reducing the threshold current density and improving device performance requires research into the fundamental material properties and defects in nitride-arsenides. Increased knowledge of the growth, combined with improved modelling, will produce a truly paradigm shifting technology for the next generation optical networks. Hence the main goal of this paper is to develop a comprehensive, fully self-consistent optical-electrical-thermal-gain model of the operation of 1.3- μm (GaIn)(NAs)/GaAs lasers. The model is especially prepared for

the PC-class microcomputers to enable their easy application, to optimize device structures and to simulate their performance characteristics.

2. Structure

Figure 1 shows the schematic structure of edge emitting (EE) (GaIn)(NAs)-GaAs SQW laser with a ridge-waveguide structure designed by NAKAHARA *et al.* [12]. It was grown on a (100)-oriented n-GaAs substrate by using gas-source molecular beam epitaxy in which a nitrogen radical was used as a nitrogen source [13]. The SQW active region consisted of a 7-nm-thick (GaIn)(NAs) strained well layer and two 150-nm-thick GaAs barrier layers. The mole fraction of both In and N in the (GaIn)(NAs) layer was characterized to be 0.3 and 0.01, respectively. Two 1.5- μm -thick $\text{Al}_{0.3}\text{Ga}_{0.7}\text{As}$ layers were used as the cladding layers in order to obtain strong electron and optical confinements [1]. The cavity length L was 800 μm . The thickness of the layer between the mesa bottom and the top of the GaAs guide layer Δ was typically 0.15 μm , so the injection current probably spread out to a larger area beyond the mesa bottom, which was approximately $S = 3.6 \mu\text{m}$ wide. Highly reflective coatings (70% and 95%) were made on the cleaved mirrors by using SiO_2 and amorphous Si.

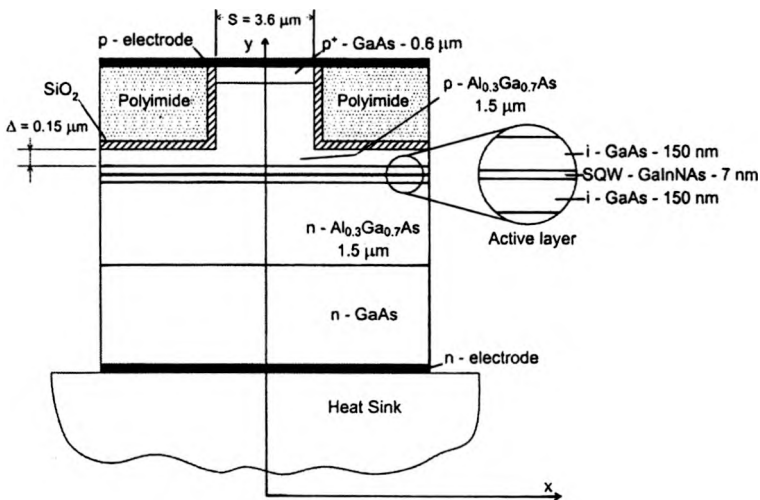


Fig. 1. SQW 1.3- μm (GaIn)(NAs) diode laser.

The cladding layers had a carrier density of $7 \times 10^{17} \text{ cm}^{-3}$. A p^+ -GaAs contact layer ($p = 3 \times 10^{19} \text{ cm}^{-3}$) was formed to decrease the contact resistance. Conventional AuZn and AuGe/Ni metallization was used for the p- and n-side contacts, respectively. The specific p-side contact resistance is assumed to be $2.4 \times 10^{-4} \Omega \text{ cm}^2$ which is a typical value for AuZn electrode.

3. Model

The computer model used to simulate RT operation of the laser under consideration consists of four principal parts:

- the optical model describing for successive radiation modes an optical field within the laser resonator,
- the electrical model characterizing both the current spreading (including carrier diffusion) between the top and the bottom contacts and the injection of carriers of both kinds into the active region,
- the thermal model characterizing the generation of a heat flux (nonradiative recombination, reabsorption of spontaneous radiation, as well as volume and barrier Joule heating) and its spreading from heat sources towards the heat sink and
- the gain model giving information about an optical gain process within the active region.

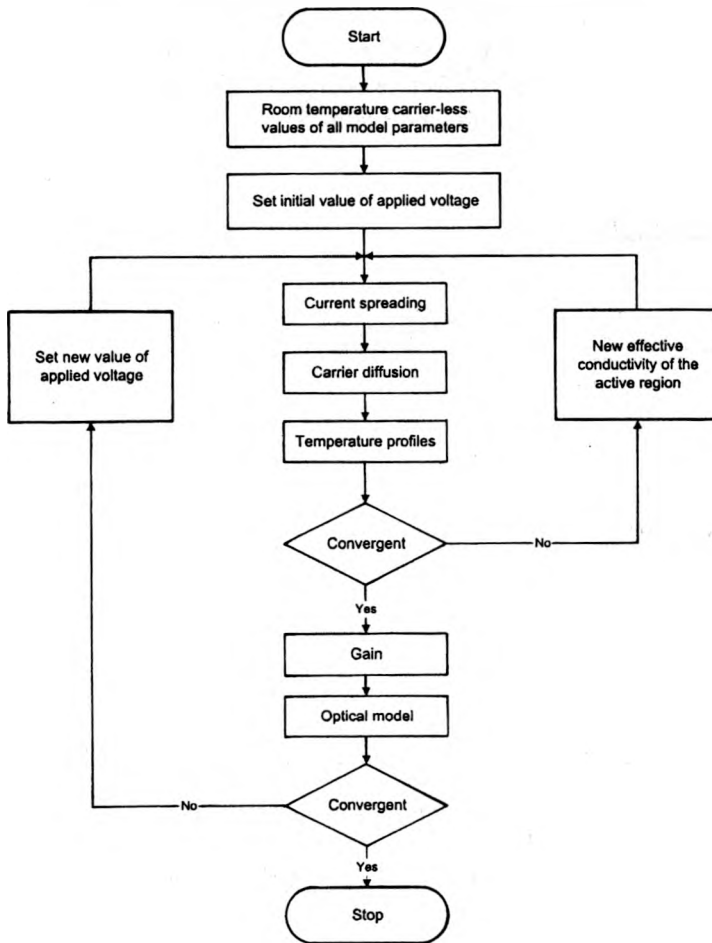


Fig. 2. Flow chart of the numerical calculation.

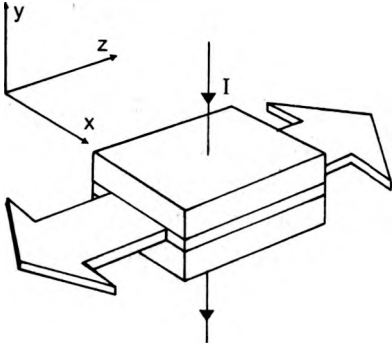


Fig. 3. Coordinate system used in the simulation.

All four singular models and most of constituting them physical processes are mutually interrelated by various important and often nonlinear interactions between individual physical phenomena, therefore self-consistent calculation algorithm is necessary. Its flow chart is schematically shown in Fig. 2. The co-ordinate system used in the simulation is presented in Fig. 3.

3.1. Optical model

Exact, comprehensive optical models of diode lasers should be vectorial ones, *i.e.* without any artificial restrictions regarding directions of the electric and magnetic fields. The method of lines (MoL) is such a semianalytical, fully vectorial optical approach. In the simulation of edge-emitting devices, MoL allows to include lateral and transversal dependences of the refractive index, carrier density, optical gain, and temperature. Analogous radial and azimuthal changes are acceptable in VCSEL modelling. In the method, discretization is performed only as long as it is necessary, whereas an analytical procedure is used otherwise. This enables obtaining accurate results with less computational effort than in case of other fully vectorial techniques, such as the finite element method or the finite difference method. What is more, the MoL approach removes the problems with the relative convergence behaviour. Non-physical or spurious modes do not appear in MoL. It makes possible the analysis of the small size structures.

In the MoL approach, the $\partial/\partial x$ derivatives are replaced in the wave equation by difference operators. This leads to the set of coupled ordinary differential equations which have to be orthogonalized. Finally, for the optical field of the m -th mode within the j -th layer, one obtains the following decoupled equation system:

$$\frac{d}{dx} \bar{\Psi}_{j,m} - k_{x,j,m}^2 \bar{\Psi}_{j,m} = 0 \tag{1}$$

with the analytical solutions

$$\bar{\Psi}_{j,m} = A_{j,m} \cosh[k_{x,j,m}(x - x_j)] + B_{j,m} \sinh[k_{x,j,m}(x - x_j)] \tag{2}$$

where $\Psi_{j,m}$ must satisfy the Helmholtz equation and the Sturm–Liouville differential equation.

To shorten the calculation time, optical behaviour of the EE device is often modelled using the effective-index method [14]. In this approach, the optically nonuniform multi-layer laser structure is replaced by an equivalent slab waveguide whose refractive-index profile is determined taking into account the geometry and the layer structure of a laser. The structure is divided into sectors of uniform refractive indices within each structure layer. Refractive indices, however, are usually different from one layer sector to another. The optical field $\Phi(x, y)$ is expressed as

$$\Phi(x, y) = \Phi_y(x) \Phi_{xy}(x, y) \quad (3)$$

where $\Phi_{xy}(x, y)$ is assumed to be slowly varying function of y (compared with $\Phi_y(x)$) in the average sense [15]. Therefore we can neglect terms containing $\partial \Phi_{xy} / \partial y$ or $\partial^2 \Phi_{xy} / \partial y^2$.

Next, the effective refractive indices n_{eff} are determined for each sector using a transfer-matrix approach proposed by BERGMANN and CASEY [16]. It enables us to determine of the $\Phi_{xy}(y)$ profile for each separate sector. Taking all sectors together, $\Phi_{xy}(x, y)$ and the $n_{\text{eff}}(y)$ profile may be obtained.

Hence the two-dimensional optical problem

$$\frac{\partial^2 \Phi}{\partial x^2} + \frac{\partial^2 \Phi}{\partial y^2} + [n_R^2(x, y)k^2 - \beta^2] \Phi = 0 \quad (4)$$

is finally converted into a much simpler one-dimensional one

$$\frac{\partial^2 \Phi_y}{\partial y^2} + [n_{\text{eff}}^2(y)k^2 - \beta^2] \Phi_y = 0. \quad (5)$$

In the above equations, n_R is the refractive index, k is the wave number and β is the propagation constant.

The idea of the transfer-matrix method used in our simulation is as follows. For each sector, the m -th mode in each j -th layer is assumed in a form of a superposition of two waves travelling in the opposite directions

$$\Phi_{j,m}(x) = A_{j,m} \exp[\gamma_{j,m}(x - x_j)] + B_{j,m} \exp[-\gamma_{j,m}(x - x_j)], \quad j = 1, 2, \dots, J \quad (6)$$

where $\gamma_{j,m}$ stands for the complex propagation constant and x_j indicates successive layer interfaces. The complex coefficients $A_{j,m}$ and $B_{j,m}$ are to be determined from continuity conditions for the electric field and its derivative at the layer edges. From the condition of the field decaying in infinity, on the other hand, the following equation with one unknown (β_m – the propagation constant) may be written for each m -th mode

$$\begin{bmatrix} 0 \\ B_{J,m} \end{bmatrix} = T_m(\beta_m) \begin{bmatrix} A_{1,m} \\ 0 \end{bmatrix} \tag{7}$$

where T_m is the transfer matrix. Hence the effective index of refraction for the m -th mode in the sector under consideration may be determined as

$$n_{\text{eff},m} = \frac{\beta_m}{k}. \tag{8}$$

Taking into account all sectors, the $n_{\text{eff},m}(y)$ profile is found.

Using the same method once more, this time in the $0y$ direction, one effective refractive index $n_{\text{eff},m}$ is found for each of the m -th mode in the whole structure. It enables us to determine, from Eq. (3), optical field profiles within the whole laser resonator for the successive m -th radiation modes, *i.e.*, for successive values of the propagation constant β_m .

3.2. Electrical model

The electrical model of the laser is based on the Laplace equation applied to all layers of the laser structure

$$\text{div}[\sigma(x, y)\text{grad}(V(x, y))] = 0 \tag{9}$$

where $\sigma(x, y)$ stands for the position-dependent electrical conductivity and $V(x, y)$ is the potential distribution. For all layers of the laser structure with the exception of the active region, the conductivity σ depends on material composition and its doping, as well as on the local temperature and the local carrier concentration. Generation and recombination phenomena within the active region are usually a source of the non-zero right-hand side of Eq. (9). They are, however, taken symbolically into account in our model with the aid of the effective conductivity σ_{pn} of the active region material. Its value is determined using the classical diode equation

$$\sigma_{\text{pn}}(x) = \frac{\beta_{\text{pn}}j_{\text{pn}}(x)d_A}{\ln[j_{\text{pn}}(x)/j_s + 1]} \tag{10}$$

where j_{pn} is the p-n junction current density. Derivation of the diode equation includes all the above mentioned phenomena in a natural way: its empirical parameters β_{pn} and j_s are dependent on the rates of carrier generation and recombination within the active region. Values of both the diode parameter ($\beta_{\text{pn}} = 8.4 \text{ V}^{-1}$) and the saturation current density ($j_s = 0.8 \text{ A/m}^2$) have been determined from experimental plots given in [17]. The parameter $d_A = 70 \text{ \AA}$ stands for the cumulative thickness of the active layer. The device is assumed to be biased by the $U \approx 1.93 \text{ V}$ voltage [17].

To obtain potential profile for the whole laser structure, it should be matched (using the self-consistent approach) with the aid of boundary conditions at all boundaries

between the layers. Then the current density distribution $j(x, y)$ may be found from the Ohm law

$$j(x, y) = -\sigma(x, y)\text{grad}[V(x, y)]. \quad (11)$$

Afterwards, the carrier density profile $n_A(x)$ within the active layer may be determined from the below threshold diffusion equation

$$D_A \frac{d^2 n_A(x)}{dx^2} - (An_A + Bn_A^2 + Cn_A^3) + \frac{j_{pn}(x)}{ed_A} = 0 \quad (12)$$

where $D_A = 10 \text{ cm}^2/\text{s}$ is the diffusion coefficient, $A = 360 \times 10^7 \text{ s}^{-1}$, $B = 25 \times 10^{-11} \text{ cm}^3/\text{s}$ and $C = 1 \times 10^{-29} \text{ cm}^6/\text{s}$ stand for the monomolecular recombination constant, bimolecular recombination constant and Auger coefficient, respectively. The values used here are estimated according to the known material and device properties.

3.3. Thermal model

In the thermal model of the laser, the heat-conduction equation

$$\text{div}[\lambda(x, y)\text{grad}(T(x, y))] = -g_T(x, y) \quad (13)$$

is solved for the whole structure. In the above equation, λ stands for the thermal conduction coefficient and g_T is the volume density of heat sources (in Wm^{-3}). Nonradiative recombination and reabsorption of spontaneous radiation is found to be a main heat source located within the active region of the laser. Additionally, the volume Joule heating in all structure layers and the barrier Joule heating in the contacts are taken into account. Copper heat sink of infinite dimensions is assumed because its sizes are two orders of magnitude larger than those of the laser itself. It has been found in this analysis that, although generally for the laser CW RT operation considered here thermal problems should not be neglected, their influence on laser operation is nearly insignificant because of considerably reduced threshold currents, which is followed by a very small heat generation.

3.4. Gain model

The gain model is based on one-electron and parabolic band approximations. The gain formula has the following form:

$$g(\hbar\omega) = \frac{e^2 \pi \hbar}{ncm_0 \epsilon_0} \int \frac{|M|^2 \rho_r}{\hbar\omega} (f_c - f_v) L \quad (14)$$

In the above equation, $\hbar\omega$ is the photon energy, M stands for the momentum matrix element, ρ_r is the reduced density of states, L describes the homogeneous broadening, and f_c and f_v are the Fermi–Dirac distributions for the conduction and the valence bands, respectively.

4. Results

Some results of our room temperature simulation are shown in successive figures. Figure 4, for example, presents RT gain spectra for successive carrier concentrations. Gain values are found to be lower than those for a typical arsenide laser, where the momentum matrix element is approximately 1.5 times greater. Apart from this, the refraction index of (GaIn)(NAs) is estimated to be equal to 3.9 for the 1300 nm wavelength. For these reasons, the threshold concentration in (GaIn)(NAs) lasers should be about twice higher than that in typical arsenide structures. According to our simulation, this value determined for the structure under consideration is equal to $4 \times 10^{-18} \text{ cm}^{-3}$.

Figure 5 presents isotherms in the neighbourhood of the active region, determined for the 1.93 V-biased (threshold voltage) reference device during RT operation. The maximum temperature (316 K) is observed near the top contact, which follows

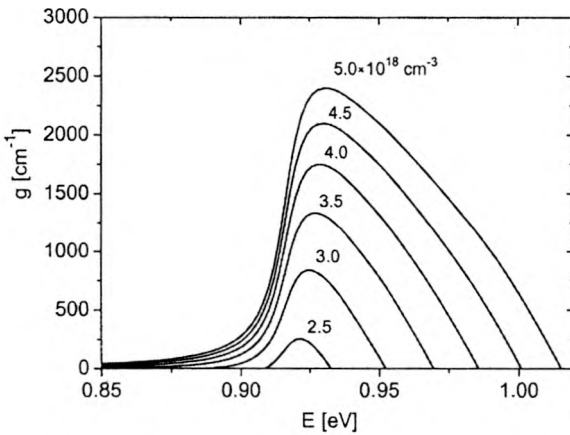


Fig. 4. RT optical gain g spectra.

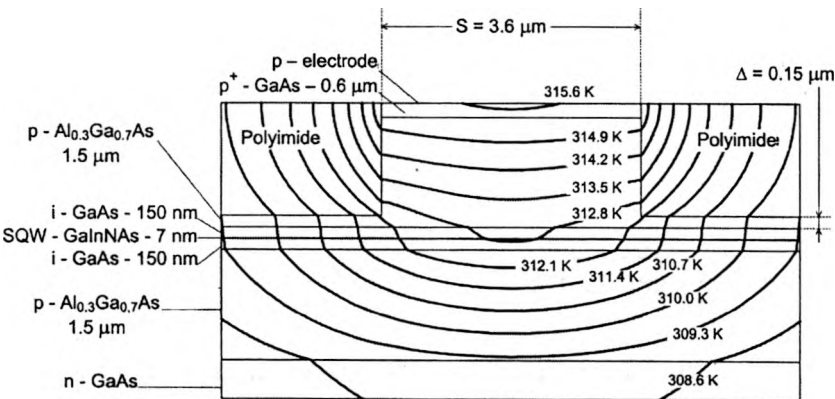


Fig. 5. Isotherms determined for the bias 1.93 V.

from the considerable amount of barrier Joule heating, as well as from confining this region by the polyimide of relatively low thermal conductivity, making heat flow difficult. The maximum temperature in the active region, on the other hand, was found to be 312 K, with the ambient temperature equal to 300 K.

Modern telecommunication lasers should operate at ambient temperatures ranging from $-40\text{ }^{\circ}\text{C}$ to $85\text{ }^{\circ}\text{C}$. From this point of view, it is important to examine the ambient temperature dependence of the structure threshold parameters. The increase in the ambient temperature to 360 K causes threefold increase in threshold current density and the maximum active region temperature increases to as much as 416 K. At the same time, the threshold voltage increases by 70% reaching 3.2 V. Threshold current increase with an increase in temperature over RT is shown in Fig. 6. The value of the T_0 parameter averaged over the whole temperature range equals to 122 K, which is consistent with the typical values found in literature. This value is almost twice as high as the one known for phosphide lasers.

Figure 7 presents the influence of the stripe-width S on both the RT CW maximal threshold current density (at the laser axis) $j_{th, max}$ and the RT CW p-n junction threshold voltage U_{th} . Minimal value of threshold current corresponds to $S \approx 6\text{ }\mu\text{m}$. However, as it is seen in the figure, the threshold voltage varies with the stripe-width,

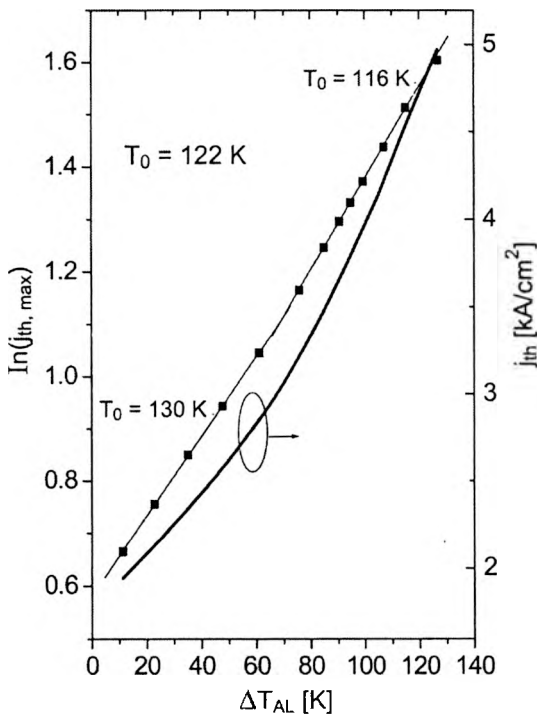


Fig. 6. Temperature dependence of the threshold current (GaIn)(NAs) diode laser density. ΔT_{AL} – increase over RT.

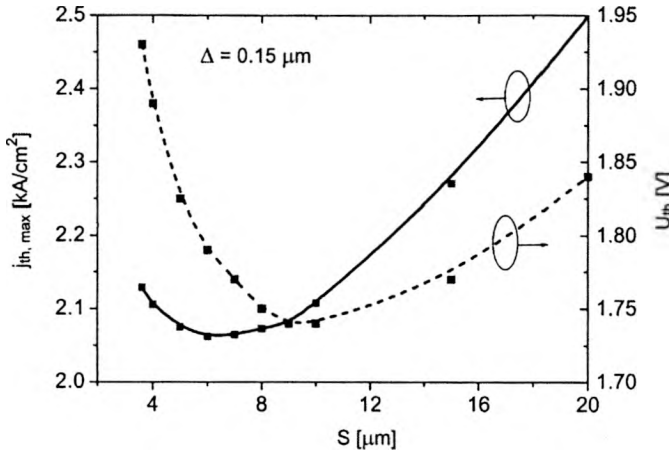


Fig. 7. Impact of the stripe-width S on the maximal threshold current density j_{th} and threshold voltage U_{th} drop at the p-n junction.

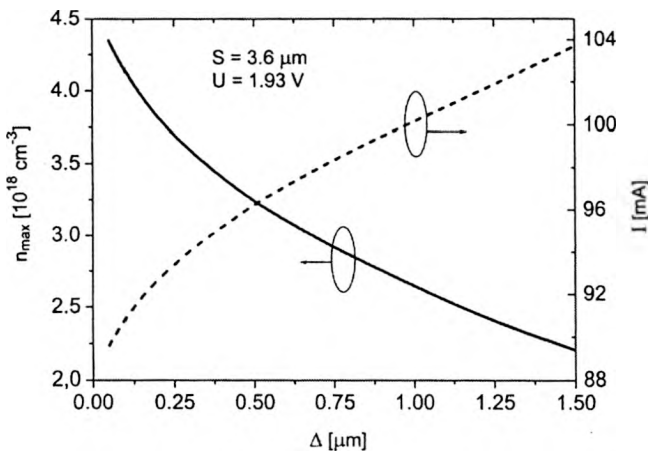


Fig. 8. Impact of the Δ parameter on the maximal current density and total operation current I .

whereas its minimum corresponds to the stripe-width $S \approx 9 \mu\text{m}$. As the current density only slightly varies with the stripe-width change from 6 to 9 μm , it seems reasonable to assume the optimal stripe-width to be 9 μm .

An impact of the construction parameter Δ (see Fig. 1) on the maximal current density and total operation current I calculated at constant supply voltage is presented in Fig. 8. The increase in I follows from an obvious decrease in the device series resistance. The current density within the active layer decreases with an increase in Δ because the current may then spread beyond the ridge structure width to a more considerable extent. In such a case the laser current is much higher causing high heat generation and hence the practical application of such a laser structure is limited.

5. Conclusions

In the present paper, the computer, self-consistent optical-electrical-thermal-gain model of the edge-emitting quantum-well 1300-nm diode GaInNAs/GaAs lasers is presented. The model takes into account all physical phenomena crucial for an operation of the diode laser with all interactions between them. The model may be used to analyse physics of the (GaIn)(NAs) QW 1300-nm arsenide-based diode lasers to better understand their performance, to simulate their operation characteristics and finally to optimise their known structures, as well as to design completely new structures corresponding to special features of 1.3- μm QW arsenide-based diode lasers.

Acknowledgments – This work has been supported by the Polish State Committee for Scientific Research (KBN), grants No 7-T11B-073-21.

References

- [1] KONDOW M., UOMI K., NIWA A., KITATANI T., WATAHIKI S., YAZAWA Y., *Jpn. J. Appl. Phys.* **35** (1996), 1273.
- [2] KONDOW M., KITATANI T., NAKATSUKA S., LARSON M.C., NAKAHARA K., YAZAWA Y., OKAI M., UOMI K., *IEEE J. Select. Topics Quantum Electron.* **3** (1997), 719.
- [3] HÖHNSDORF F., KOCH J., AGERT C., STOLZ W., *J. Cryst. Growth* **195** (1998), 391.
- [4] POLIMENI A., CAPIZZI M., GEDDO M., FISCHER M., REINHARDT M., FORCHEL A., *Appl. Phys. Lett.* **77** (2000), 2870.
- [5] HETTERICH M., DAWSON M.D., EGOROV A.YU., BERNKLAU D., RIECHERT H., *Appl. Phys. Lett.* **76** (2000), 1030.
- [6] NAKAHARA K., KONDOW M., KITATANI T., LARSON M., UOMI K., *IEEE Photon. Technol. Lett.* **10** (1998), 487.
- [7] EGOROV A., BERNKLAU D., LIVSHITS D., USTINOV V., ALFEROV Z., RIECHERT H., *Electron. Lett.* **35** (1999), 1643.
- [8] SATO S., SATOH S., *Electron. Lett.* **35** (1999), 1251.
- [9] HÖHNSDORF F., KOCH J., LEU S., STOLZ W., BORCHERT B., DRUMINSKI M., *Electron. Lett.* **35** (1999), 571.
- [10] ELLMERS C., HÖHNSDORF F., KOCH J., AGERT C., LEU S., KARAIKAI D., HOFMANN M., STOLZ W., RÜHLE W.W., *Appl. Phys. Lett.* **74** (1999), 2271.
- [11] REINHARDT M., FISCHER M., KAMP M., HOFMANN J., FORCHEL A.W., *IEEE Photon. Technol. Lett.* **12** (2000), 239.
- [12] NAKAHARA K., KONDOW M., KITATANI T., LARSON M.C., UOMI K., *IEEE Photon. Technol. Lett.* **10** (1998), 487.
- [13] KONDOW M., UOMI K., HOSOMI K., MOZUME T., *Jpn. J. Appl. Phys.* **33** (1994), L1056.
- [14] CHIANG K.S., *Appl. Opt.* **25** (1986), 348.
- [15] LIU G.T., STINTZ A., LI H., MALLOY K.J., LESTER L.F., *Electron. Lett.* **35** (1999), 1163.
- [16] BERGMANN M.J., CASEY H.C. JR., *J. Appl. Phys.* **84** (1998), 1196.
- [17] KONDOW M., KITATANI T., NAKAHARA K., TANAKA T., *Jpn. J. Appl. Phys.* **38** (1999), L1355.

Received May 13, 2002